Magneto-Optical Measurements of the Pigments in Fully Active Photosystem II Core Complexes from Plants †

ARTICLE *in* BIOCHEMISTRY · FEBRUARY 2002

Impact Factor: 3.02 · DOI: 10.1021/bi0111202 · Source: PubMed

7 AUTHORS, INCLUDING:

Elmars Krausz
Australian National University
218 PUBLICATIONS **3,405** CITATIONS

SEE PROFILE

Ron J Pace
Australian National University
95 PUBLICATIONS **3,409** CITATIONS

SEE PROFILE

Magneto-Optical Measurements of the Pigments in Fully Active Photosystem II Core Complexes from Plants†

Paul J. Smith,‡,§,|| Sindra Peterson,‡,§,||,⊥ Vanessa M. Masters,§ Tom Wydrzynski,|| Stenbjörn Styring,⊥ Elmars Krausz,*,§ and Ron J. Pace*,‡

Faculties Chemistry, Research School of Chemistry, and Research School of Biological Sciences, The Australian National University, Canberra, ACT 0200, Australia, and Department of Biochemistry, Chemical Center, Lund University, S-22100 Lund, Sweden

Received May 31, 2001; Revised Manuscript Received December 7, 2001

ABSTRACT: Preparation of a minimum PSII core complex from spinach is described, containing four Mn per reaction center (RC) and exhibiting high O_2 evolving activity [~4000 μmol of O_2 (mg of chl)$^{-1}$ h^{-1}]. The complex consists of the CP47 and CP43 chlorophyll binding proteins, the RC D1/D2 pair, the cytochrome b_{559} subunits, and the Mn-stabilizing psbO (33 kDa) protein, all present in the same stoichiometric amounts found in the parent PSII membranes. Several small subunits are also present. The cyt b_{559} content is 1.0 per RC in core complexes and PSII membranes. The total chlorophyll content is 32 chl *a* and <1 chl *b* per RC, the lowest yet reported for any active PSII preparation. The core complex exhibits the characteristic EPR signals seen in the S_2 state of higher plant PSII. A procedure for preparing low-temperature samples of very high optical quality is developed, allowing detailed optical studies in the S_1 and S_2 states of the system to be made. Optical absorption, CD, and MCD spectra reveal unprecedented detail, including a prominent, well-resolved feature at 683.5 nm (14 630 cm^{-1}) with a weaker partner at 187 cm^{-1} to higher energy. On the basis of band intensity, CD, and MCD arguments, these features are identified as the exciton split components of P680 in an intact, active reaction center special pair. Comparisons are made with solubilized D1/D2/cyt b_{559} material and cyanobacterial PSII.

Photosystem II (PSII)[1] is the large multisubunit protein complex found in all oxygenic photosynthetic organisms. PSII catalyzes the oxidation of water to molecular oxygen, within the thylakoid membranes of higher plants and algae, as well as cyanobacteria (*1*−*3*).

Central to PSII is a membrane-incorporated core complex comprising the reaction center (RC) D1 and D2 proteins, the inner chlorophyll *a* (chl *a*) binding proteins CP43 and CP47, the cytochrome b_{559} (cyt b_{559}) heterodimer, and several small peptides (<10 kDa) of as yet unknown function (*4*). The D1/D2 heterodimer contains the photo-oxidizable special chlorophyll pair (P680) as well as the pigment components [two pheophytin *a* (pheo *a*), two accessory and two peripheral chl *a*] associated with primary light-driven charge separation across the thylakoid membrane. The D1 peptide appears to ligate the Mn cluster responsible for catalytic water oxidation and binds an extrinsic, water-soluble protein (33 kDa, psbO) at the luminal cytoplasmic face, which helps stabilize this Mn center (*5*).

Major differences between the PSII structures in higher plants and cyanobacteria involve the outer light-harvesting (LHC) protein assemblies and Mn-stabilizing peptides (*6*). Both higher plants and cyanobacteria have two extra (in addition to the 33 kDa protein) extrinsic, lower molecular weight Mn-stabilizing proteins (23 and 16 kDa proteins in plants, cyt c_{550}, and PSII-U in cyanobacteria).

A number of procedures have been reported to isolate core complexes from cyanobacteria and plants. The detergent-solubilized species obtained exhibit varying degrees of functional (water splitting) intactness [e.g., see (*7*) and references cited therein, (*8*−*18*)]. Recently, PSII preparations from thermophilic cyanobacteria with high specific turnover activity [up to 5000 μmol of O_2 (mg of chl)$^{-1}$ h^{-1}]

† This work was supported by the Australian Research Council (grant to R.J.P.), the Swedish Natural Science Research Council (grant to S.S.), the K. and A. Wallenberg Foundation (grant to S.S.), the Swedish Energy Authority (grant to S.S.), and the Wenner−Gren Foundations (fellowship to S.P.).

* To whom correspondence should be addressed. E.K.: phone +61 2 6125 3577; fax +61 2 6125 0750; email krausz@rsc.anu.edu.au. R.J.P.: phone +61 2 6125 4546; fax +61 2 6125 8997; email Ron.Pace@anu.edu.au.

‡ Faculties Chemistry, The Australian National University.

§ Research School of Chemistry, The Australian National University.

|| Research School of Biological Sciences, The Australian National University.

⊥ Department of Biochemistry, Lund University.

[1] Abbreviations: BBY, solubilized PSII membrane fragments; BIS-TRIS, [bis(2-hydroxyethyl)amino]tris(hydroxymethyl)methane; CD, circular dichroism; CP29/43/47, chlorophyll binding proteins of 29, 43, and 47 kDa molecular mass, respectively; chl, chlorophyll; cyt, cytochrome; D1/D2/b559, solubilized PSII containing the D1 and D2 proteins and cyt b_{559}; DCMU, 3-(3,4-dichlorophenyl)-1,1-dimethylurea; β-d-DDM, *n*-dodecyl β-D-maltoside; EPR, electron paramagnetic resonance; FPLC, fast-performance liquid chromatography; HPLC, high-performance liquid chromatography; IR, infrared; LHC, light-harvesting complex; LiDS, lithium dodecyl sulfate; MCD, magnetic circular dichroism; MES, 2-(*N*-morpholino)ethanesulfonic acid; NIR, near-infrared; pheo, pheophytin; PPBQ, phenyl-*p*-benzoquinone; PSII, photosystem II; Q_A, primary quinone acceptor; Q_B, secondary quinone acceptor; RC, reaction center; TRIS, tris(hydroxymethyl)aminomethane; VB, visual basic.

10.1021/bi0111202 CCC: $22.00
Published on Web 00/00/0000 PAGE EST: 9

have been successfully crystallized (*17*−*20*).

Comparably purified PSII core complex material from higher plants has often shown much lower specific activity [<1000 μmol of O_2 (mg of chl)$^{-1}$ h^{-1}] (*9, 11, 12*), unless some of the LHC components are retained (*12, 21*). Until recently, even the chlorophyll stoichiometry of the PSII core complex was uncertain. Earlier estimates suggested up to ∼60 chl *a* per reaction center (*1*). It is now clear from both pigment analysis (*10, 12, 17*), and particularly from medium-resolution 2D and 3D crystallography on higher plant (*22, 23*) and cyanobacterial systems (*20*), that the total chl *a* content of the core complex (i.e., of CP47+CP43+D1/D2 reaction center) is 32−35 chl *a*, with 2 pheophytins *a* per reaction center.

The protein−pigment organization of the D1/D2 region of PSII is now known to closely resemble the purple bacterial reaction center structure (*20, 22, 24, 25*). Nevertheless, a detailed interpretation of the electronic structure and interaction of the pigment components of the PSII reaction center is still controversial [e.g., (*26*−*29*)]. This is mainly due to a lack of distinct features within the relatively compact spectral region identified with the PSII reaction center, as compared to spectra of the bacterial system, where interaction splittings are much greater.

Most optical studies addressing the dynamics of energy transfer and pigment coupling in PSII have employed highly solubilized D1/D2/cyt b_{559} particles (D1/D2/b_{559}) (*30*). Although functional in charge separation, the reaction center environment in these preparations is heterogeneous (*31*) and substantially altered from its native, in vivo state, having lost all peripheral membrane and cytoplasmic protein components as well as the Mn cofactors.

Recently, we have embarked on an extensive program of variable-temperature absorption, emission, circular dichroism (CD), and magnetic circular dichroism (MCD) spectroscopy of enzymatically functional PSII core complexes from higher plants and cyanobacteria. This required the development of preparative protocols for functionally intact PSII core complexes from higher plants having a minimum LHC pigment contamination. It also required the evolution of techniques by which samples of high optical clarity and isotropy could be prepared at low temperatures.

Here we describe this preparative procedure, which is the first for PSII core complexes from higher plants to exhibit very high catalytic activity levels, comparable to those attainable from thermophilic bacterial sources. Low-temperature (<10 K) optical absorbance studies show that the chl *a* Q_y region displays very well resolved pigment features, significantly narrower than those observed in D1/D2/b_{559} preparations.

MATERIALS AND METHODS

PSII Sample Preparation. In basic outline, the present procedure for PSII core complex preparation from spinach follows established methods. Its unique success appears to derive from careful attention to a number of details in the total process, from PSII membrane preparation through to column separation of the solubilized core complex material. The key features are all given here.

All procedures of PSII membrane and core complex preparation were undertaken under dim green light and at 4 °C unless otherwise indicated. PSII membrane samples were prepared according to Smith et al. (*32*). Protease inhibitor was not used. Bovine serum albumin (BSA fraction IV, Sigma) was added as a sacrificial protein to all buffers prior to the Triton X-100 detergent solubilization step. The solubilized membrane samples were washed once in 50 mM MES, pH 6.0, 50 mM NaCl, and 5 mM $MgSO_4$ to remove Triton detergent. The solubilized membrane samples were stored at 12−16 mg of chl/mL in a buffer containing 0.4 M sucrose, 10 mM NaCl, 15 mM $MgCl_2$, and 20 mM MES, pH 6.0 (NaOH), at −85 °C.

Preparation of PSII core complexes followed, in principle, the procedure of van Leeuwen et al. (*9*). All buffers used in the PSII core complex preparation were prefiltered using a 0.45 μm filter. This removed particulates, which may affect the FPLC process. The PSII membrane samples (∼30−40 mg of total chlorophyll) were diluted to 2.0 mg/mL in a system buffer consisting of 0.4 M sucrose, 20 mM $MgCl_2$, 10 mM $MgSO_4$, 5 mM $CaCl_2$, 0.3 mg/mL β-d-DDM, and 20 mM BIS-TRIS, pH 6.5 (HCl). The diluted sample was solubilized by stirring for 10 min at 25 °C in darkness with β-d-DDM (as a 10% detergent solution in system buffer) to a final concentration of ∼71.5 mg of β-d-DDM/mg of chl (1.25% β-d-DDM w/v in the solubilization). The solubilized membranes were centrifuged at 17000*g* at 15 °C for 15 min. The supernatant was then placed on ice in darkness to halt solubilization. The PSII core isolation procedure followed the perfusion chromatography protocol according to Roobal-Bóza et al. (*11*) using a Poros HQ 20 column medium, self-packed to a pressure of <2 MPa. Flow rates were maintained at about 2 column volumes per minute while maintaining a column backpressure below 2 MPa. The PSII core complexes were eluted following the initial LHC peak with system buffer plus 80 mM $MgSO_4$, using a 2 min linear gradient from the system buffer to the elution buffer. The eluted fractions containing the PSII core complexes were pooled and concentrated using Centriprep centrifugal concentrators (Amicon, 10 kDa MW cutoff) and stored (1−3 mg of chl/mL in the elution buffer) at −85 °C until used. If more than one column run was undertaken, each FPLC procedure was run after column regeneration consisting of 15 column volumes of 1 M NaCl, followed by 15 column volumes of ultrapure H_2O, followed by the preequilibration step of 15 column volumes of system buffer. The yield of chl in the eluted PSII core complex samples was 3−5% of the total chl in the starting PSII membranes prior to solubilization.

All chl content and chl *a*/*b* ratios were determined using buffered 80% acetone as a solvent, following the protocol of (*33*).

Oxygen Evolution. Oxygen evolution measurements employed a Hansatech electrode system with PPBQ and $K_2Fe(CN)_6$ (both 200 μM) as electron acceptors. Acceptor side intactness was examined by addition of DCMU (50 μM) to the oxygen electrode measurement chamber.

Pigment and Metal Analysis. PSII samples were diluted to 40 μM chl concentration in buffered 80% acetone solution (HPLC grade, pH 7.8) and centrifuged at 10000*g* to remove particulates and detergent. HPLC pigment analysis was undertaken according to (*34*).

Mn determination was performed by acidifying the PSII material in 1 M HCl and quantitating the resulting Mn '6 line' electron paramagnetic resonance (EPR) signal at 10 K

against EPR standards. This also allowed an estimate of the unbound Mn content (i.e., EPR-visible species) in the intact PSII material (see Figure 5).

Polypeptide Analysis. Polyacrylamide gel electrophoresis employed a 10−17% polyacrylamide gradient gel system (*30*) with 6 M urea in the resolving gel and peptide solubilization buffer and Coomassie Blue staining. Western blot analysis and antibody staining were carried out by T. Hundall and C. Spetea (Linköping University, Sweden) using procedures established in their laboratory (*11*).

EPR Spectroscopy. X-band EPR experiments were carried out on a Bruker ESP300E spectrometer using a microwave frequency of 9.42 GHz (*35*). Buffer and sample conditions for the PSII core samples used are described in the figure legends. Samples were examined with dilution in both system (10 mM $MgSO_4$) and elution (90 mM $MgSO_4$) buffers. No differences in the turnover capabilities of the EPR samples were observed based on the presence of up to 90 mM $MgSO_4$. The presence of 30 mM Cl^- in the elution buffer appears to protect the PSII core samples from SO_4^{2-} inhibition with the 17 and 23 kDa extrinsics removed during the core isolation procedure.

Samples were illuminated for 12−20 s in a N_2 flow cryostat with a 250 W lamp at 255 K, using blue or green filtered light and a 10 cm water path IR filter, to induce S_1-to-S_2 turnover (generating the multiline form of the S_2 state). The S_2 samples were subsequently illuminated at 145 K using a 715 nm cutoff filter in the far-red/near-infrared (NIR) for 15 min to generate the $g \approx 4.1$ form of the S_2 state. The terminal acceptor site of the PSII cores prepared by the van Leeuwen (*9*) protocol is known to be unoccupied, with Q_B missing. The illumination temperature allows full turnover of the PSII cores from the S_1 to the S_2 state while minimizing formation of carotenoid or chlorophyll radicals. These were observed to be generated using illumination temperatures below ∼235 K (data not presented). By quantitation of the S_2 multiline EPR signal, sample turnover was observed to be 0.8−1.0 multiline spin formed per RC using the >255 K illumination protocol. Spin quantitation was done by double integration of $S_2 - S_1$ difference spectra, via comparison against the signal from Y_D^{ox} and EPR standards ($CuSO_4$).

Optical Spectroscopy. Thawed samples were diluted to ∼0.3 mg of chl/mL in the elution buffer and dark-adapted at 20 °C for 2 min. Then 1:1 ethylene glycol/glycerol was added to give a final polyalcohol concentration of 40% (v/v), and the sample was syringed into a quartz windowed cell (∼100 μL) of path length 1 mm. This was mounted onto a sample rod and lowered into an Oxford Instruments Spectromag 4 (SM4) cryostat. Glasses of good optical quality were obtained by cooling the solution (over approximately 40 s) from room temperature to 4 K. The absorption and CD, or the absorption and MCD, were collected *simultaneously* on an apparatus designed and constructed in our laboratory (*36*). The MCD measurements were collected upon application of a 5 T magnetic field to the sample.

RESULTS

PSII Core Complex Analysis. Table 1 summarizes the analytical data on our PSII core complex material. The observed range in catalytic activity generally reflects variation in the activity of the starting PSII membrane material.

Table 1: Activity/Component Analyses[a] for Core Complexes and PSII Membrane Particles

	core complex	PSII membranes
activity [μmol of O_2 (mg of chl)$^{-1}$ h^{-1}]	3700−4300	600−800
+ 50 μM DCMU	< 5	∼ 0
component		
pheophytin *a*	2.00	2.00
chlorophyll *a*	32 ± 1	134 ± 2
chlorophyll *b*	0.8 ± 0.2	62 ± 1
β-carotene	7 ± 1	9 ± 1[d]
Mn	4.5 ± 0.5[b]	∼5
cyt b_{559}	1.0 ± 0.05[c]	1.0 ± 0.2[e]

[a] All component stoichiometries are given per 2.00 pheo *a*, assumed to represent one PSII reaction center. [b] Bound content, excluding superficially associated Mn^{2+} (see Figure 5, Materials and Methods). [c] Determined by quantitative scaling of the MCD spectra (see text). [d] β-Carotene only. Excludes xanthophylls and lutenes. [e] Determined by an analysis of the MCD spectra of PSII membranes and the relative intensities of the cyt b_{559} subunit to core complex bands in gels (see text).

Rates of order 4000 μmol of O_2 (mg of chl)$^{-1}$ h^{-1} are significantly higher than any previously reported for higher plant derived PSII material. This activity was almost completely inhibited by 50 μM DCMU. We find a total of 32 chl *a* and 7 carotenoids (β-carotene only) per reaction center, assuming the standard 2.00 pheo *a* stoichiometry for the latter. In addition, we find 4.5 ± 0.5 Mn per 32 chl *a*, which is substantially higher than the generally reported Mn/chl ratio in cyanobacterial core complex preparations (*7*, *8*, *10*, *14*).

A value of 32 chl *a* per reaction center is very close to the number observed (or inferred) from crystallographic studies (*20*, *22*, *23*) on higher plant or cyanobacterial core complexes (i.e., CP47, 14 chl; CP43, 12−14 chl; RC, 6 chl; 32−34 chl total). The carotenoid content (∼7 per reaction center) is virtually the same as that reported by Hankamer et al. (*12*) for dimeric PSII core complexes. We presume that our material is in this form, although this has not been directly determined.

We find a single cyt b_{559} per 32 chl *a*, by low-temperature MCD (see below). The oxidized and reduced forms are easily distinguished. The cytochrome is >95% oxidized in the buffer/cryoprotectant medium used to glass the core samples used for optical study. A single cyt b_{559} per reaction center is consistent with earlier determinations on cyanobacteria (*8*, *10*) and the recent PSII crystal structure for *S. elongatus* (*20*).

Figure 1 shows a comparison of gel patterns for detergent-solubilized core complex and the parent PSII particles. Notable is the near-absence of any LHC chl pigment proteins in the core complex, but the essentially quantitative retention (relative to the CP43 and CP47 bands) of the 33 kDa Mn-stabilizing protein. The 23 and 16 kDa extrinsic proteins are absent, as expected. Comparison with the gel patterns from earlier reported higher plant derived PSII core complex preparations [e.g., (*12*)] suggests that the high activity of the present material derives from its retention of the 33 kDa protein in functionally attached form.

Western blotting and antibody staining indicate that the faintly discernible feature below 30 kDa apparent molecular mass in the core complex gel pattern contains CP29. This contamination is <10 mol % (per complex) based on the chl *b* content (Table 1) and absorption spectra (Figure 2

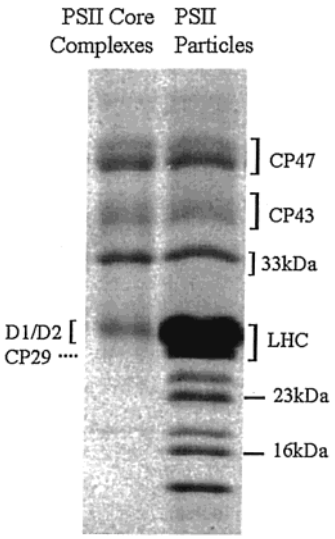

FIGURE 1: Gel comparison of peptide bands (above ~12 kDa) from PSII core complexes and the PSII membrane material from which the complexes were made. The gels were loaded with approximately equal reaction center protein content. The CP43 band is broad, as is frequently seen in higher plant PSII [e.g., (*12, 21*)], possibly due to variable phosphorylation levels. Essentially stoichiometric retention of the 33 kDa Mn stabilizing protein in the core complexes is evident, with total loss of the 16 and 23 kDa extrinsic proteins. The band labeled CP47 shows two components of slightly differing apparent molecular mass. Both are confirmed to contain CP47 by peptide fragment sequencing. This behavior of CP47 has been seen previously (*69*). A comparison of Figure 1 above and Figure 5 in (*69*) suggests that the relative distribution of CP47 between the two forms is variable.

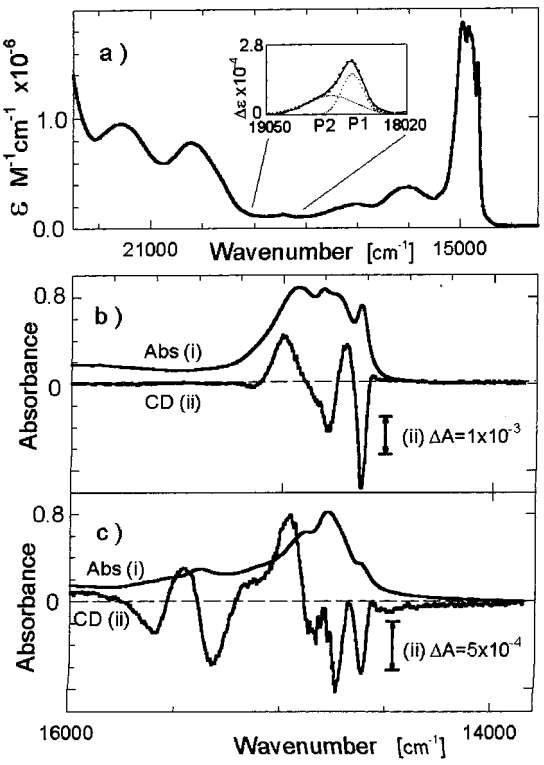

FIGURE 2: (a) Visible/NIR region absorption spectrum of PSII core complexes. The inset shows the pheophytin Q_x region, with active (P1) and inactive (P2) branch chromophore bands indicated. The extinction coefficient (per reaction center) scale assumes a dipole strength, *D*, for the chl *a* $Q_y(0,0)$ band of 19.1 D (*44*) and pigment compositions from Table 1. (b, c) Absorbance and CD spectra of the chlorophyll Q_y region of core complexes and PSII particles, respectively. All spectra are recorded at 1.9 K in a glassed matrix as described under Materials and Methods.

below). Low molecular weight gels and blotting (not shown) also indicate the presence of several small PSII subunits, including psbW and the α subunit of cyt b_{559}.

Absorbance and CD. Figure 2a shows the visible−NIR absorption spectrum of the PSII core complex in the dark-adapted (S_1) state at 1.5 K. The pheophytin Q_x region is shown in detail as an inset. The inset shows a combination of active (pheo 1) and inactive branch (pheo 2) chromophore bands, which are distinguished by differential electrochromic shifts following light-induced turnover to the $Q_A^-S_2$ state (*37*).

Figure 2b shows the chlorophyll Q_y region in detail, together with the corresponding CD spectrum. The prominent feature at 14 630 cm^{-1} (683.5 nm) has a line width of only 45 cm^{-1} and a distinct negative CD band. The same feature is present in the absorption and CD of intact PSII particles, with approximately the same intensity (per reaction center) and line width (Figure 2c).

The absorption envelope in Figure 2b consists of two partially overlapping regions: a broad approximately Gaussian band centered around 14 900 cm^{-1} (~670 nm) which is responsible for most of the total intensity (70−80%) and a spectrally compact but structured region toward the red which includes the 14 630 cm^{-1} band. The structure observed in this region is more resolved than that seen in D1/D2/b_{559} particles [e.g., (*28*−*31, 38, 39*)] or isolated CP43, CP47 complexes [e.g., (*40*−*42*)].

Consistent with the gel pattern results in Figure 1, a comparison of the Q_y absorption and CD envelopes in Figure 2b,c shows little, if any, detectable LHC spectral contribution in the core complexes. This is particularly evident in the CD spectra, where LHC chl *b* contributions in the 15 000−16 000 cm^{-1} region are below the noise level in the CD spectra of the core complexes.

MCD. Figure 3a shows the visible/NIR absorption and MCD spectra of the PSII core complexes at 1.5 K. The MCD spectrum is the first reported for functional oxygen-evolving PSII material. It is dominated by the chl *a* Faraday *B*-term (diamagnetic and temperature-independent) (*43*). The sign is positive for the band origin $Q_y(0,0)$ transition and negative for the $Q_y(0,1)$ (*44*). For the $Q_y(0,0)$ band of an isolated chl *a* chromophore, the characteristic property B_0/D_0 (MCD moment/transition moment) is proportional to $\Delta\epsilon_M/\epsilon$ (molar ellipticity/extinction coefficient), and the latter has been determined to be 5.53×10^{-4} T^{-1} (*44*).

Figure 3b shows detailed absorption and MCD spectra in the chl Q_y region. The observed spectra have been scaled (according to the above $\Delta\epsilon_M/\epsilon$ ratio for a 5 T field) to display a marked variation in the magnitude of the MCD [Figure 3b(ii)], compared to absorption [Figure 3b(i)], across the band.

For isolated chl *a*, the Q_y band shapes in absorption and MCD are the same to a good approximation (*44*). In a distribution of noninteracting chl *a* chromophores, the ΔA(MCD) will be proportional to the absorbance, *A*, at any point. In the high-energy region of the core complex Q_y envelope, the chl *a* do indeed behave, with respect to their MCD, as a collection of monomeric chromophores. However, the (lower energy) reaction center region displaying resolved

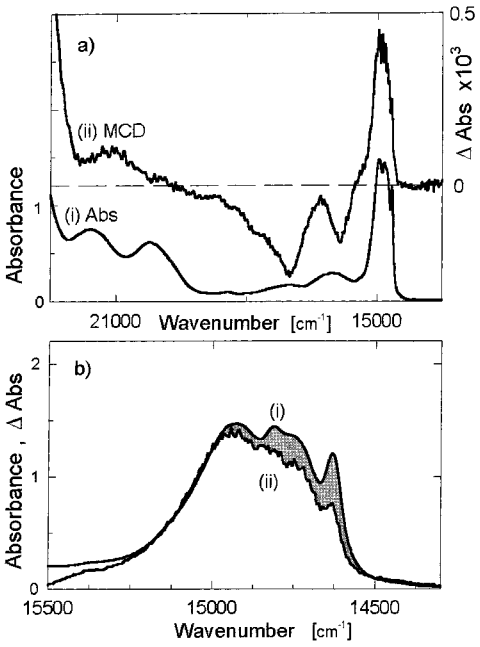

FIGURE 3: (a) Comparison of absorption and MCD spectra for PSII core complexes over the same observation range as in Figure 2a. Sharp derivative features near 18 000 cm^{-1} are undetectable, indicating an essential absence of the reduced form of cyt b_{559} (see text). (b) Comparison of absorbance and MCD spectra in the chlorophyll Q_y region. The MCD intensity has been scaled as described in the text. The filled area corresponds to the apparent MCD deficit (see text). The temperature is 1.5 K, field 5.0 T. Sample conditions as in Figure 2.

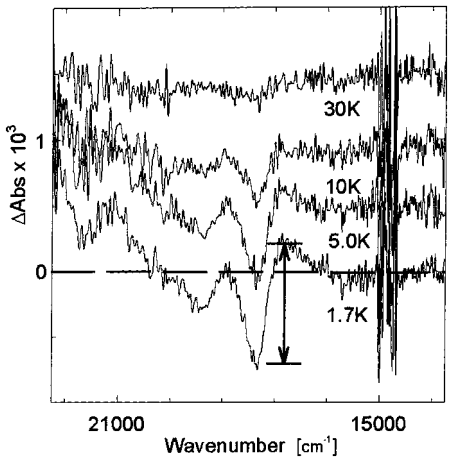

FIGURE 4: Temperature-dependent component of MCD spectra of PSII complexes over the frequency range of Figure 2a. The MCD presented is that at the observation temperature minus that at 60 K. Increased noise in the chl Q_y region is inherent and arises from the low light levels in regions of high absorbance. Field 5 T and sample conditions as in Figure 2. The bar shows points between which $\delta\Delta\epsilon_M$ was measured (see text). The extinction coefficient scale is established as described in Figure 2, from simultaneously acquired MCD and absorption data.

structural features exhibits a significantly smaller $\Delta A/A$ ratio compared to isolated chl *a*. This 'MCD deficit' (filled region in Figure 3b) is most pronounced at the prominent 14 630 cm^{-1} (683.5 nm) feature, where the $\Delta\epsilon_M/\epsilon$ has fallen to approximately half that for monomeric chl *a*.

Some of the observed MCD deficit may originate from pheophytin. We note that the peak $\Delta\epsilon/\epsilon$ for (isolated) pheo *a* is ~40% that of (isolated) chl *a*. However, the total deficit observed in Figure 3b corresponds to a total of 3−4 chl *a* molecules. As the absorption strength (in integrated intensity) of pheo *a* in the Q_y region is 74% that of chl *a*, it follows that 2 pheo *a* can account for only ~1.4 chl *a* deficit equiv. The remaining deficit we attribute to a reduction of chl *a* MCD associated, phenomenologically, with interchromophore coupling. This is discussed further below.

Other features readily observable in the low-temperature MCD spectra are those associated with the heme α-band region (17 000−18 000 cm^{-1}, 550−560 nm) of low-spin cyt b_{559}, in both the Fe^{II} and Fe^{III} forms (Figure 3a). Fe^{II} cytochrome has a strong, sharp Faraday *A*-term feature in the α-band region, with a characteristic derivative shape (*45*). In the solubilized PSII core complexes studied here, such derivative-shaped signals from the reduced form are not seen (Figure 3a), establishing that >95% of the cytochrome is oxidized. (This is supported by EPR; see Figure 5 and below.) A Fe^{III} MCD band is temperature-dependent, displaying $1/T$ temperature dependence (Faraday *C*-term behavior). This is distinctly different from that associated with diamagnetic species absorbing in the region (chl, pheo, and Fe^{II} cytochrome).

Figure 4 shows the temperature-dependent MCD spectra of the PSII core complex over the same wavelength range as in Figures 2a and 3a. The spectra closely resemble those of Fe^{III} heme proteins in all relevant features (*45*). MCD spectral features around 17 000−18 000 cm^{-1} show relatively little variation in Fe^{III} heme proteins, in both shape and absolute intensity (*45*−*48*). The $\delta\Delta\epsilon_M$ value between the 17 400 cm^{-1} trough and the 16 800 cm^{-1} peak (at 4 K and 5 T, see Figure 4) varies only weakly with heme ligand type [$\delta\Delta\epsilon_M = 1.1 \times 10^3$ $M^{-1}cm^{-1}$ (mono his), 1.3×10^3 M^{-1} cm^{-1} (his-his), $(1.3-1.5) \times 10^3$ M^{-1} cm^{-1} (his-met)]. Although cyt b_{559} has never itself been measured, the spectral shape in Figure 4 is indistinguishable from that of the bi-his-ligated cyt *c*3 center (*46*), for which $\delta\Delta\epsilon_M = 1.30 \times 10^3$ M^{-1} cm^{-1} (4.2 K and 5 T). Using this value, the cyt b_{559}/reaction center stoichiometry given in Table 1 is obtained.

In analogous MCD spectra of PSII membrane particles (not shown), both reduced and oxidized cytochrome signals are seen. Again using literature MCD $\Delta\epsilon_M$ values (*45*), the total cytochrome content sums to one per reaction center, but the balance between the oxidized and reduced fractions is variable between membrane samples.

EPR. Functionally intact PSII exhibits two well-known low-temperature EPR signals arising from the Mn catalytic site: the multiline signal centered at $g \approx 2$ and a signal at $g \approx 4.1$. Both are formally associated with the S_2 state (*5*). The S_2 state is obtained by single electron turnover from the dark-stable S_1 state. Although EPR signals from all four (S_0, S_1, S_2, S_3) quasi-stable intermediates of the Mn cluster have now been identified (*49*), the S_2 multiline and $g \approx 4.1$ signals are the best characterized and are easily generated by well-established protocols of low-temperature continuous illumination.

Figure 5 shows the low-temperature EPR spectra of the core complex in the S_1 (dark state) and S_2 states. The S_1 state spectrum clearly shows signals at $g \approx 2.26$, 2.97 arising from low-spin Fe^{III} cyt b_{559}, as well as background rhombic Fe^{III} ($g \approx 4.3$) normally present in photosystem preparations (*50*). Green or blue illumination (see Materials and Methods)

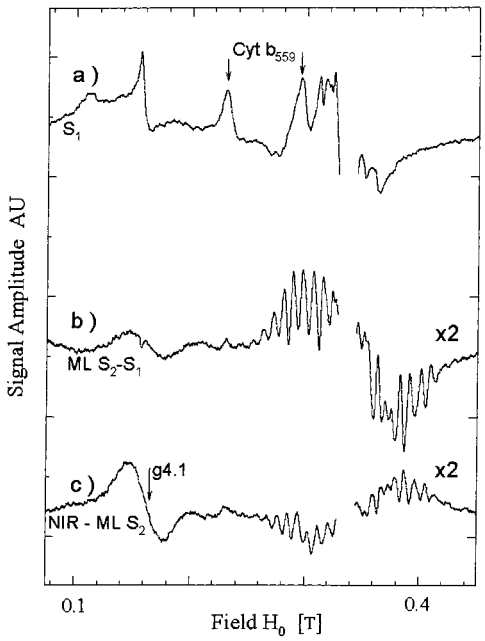

FIGURE 5: EPR spectra of PSII core complex material in the same cryoprotectant/buffer used for optical studies (see Materials and Methods, 1 mg of chl/mL final sample concentration). (a) S_1 represents the dark state sample with downfield peaks of oxidized, low-spin cyt b_{559} as indicated (arrows). Peaks with 9 mT spacing in the $g = 2$ region are from unbound Mn^{2+} and correspond to ~0.3 Mn^{2+} per reaction center. The radical region close to $g = 2$ [mainly oxidized tyrosine, Y_D^{ox} (*5*)] has been omitted. (b) ML S_2-S_1 is the difference spectrum for the multiline form of the S_2 state minus the S_1 state (see Materials and Methods). (c) NIR − ML S_2 is the difference spectrum corresponding to partial conversion (~50%) of the multiline to the $g \approx 4.1$ form of the S_2 state by low-temperature NIR illumination (see Materials and Methods). The multiline region has negative phase, showing loss of signal. Vertical scaling of (b) and (c) is twice that of (a). EPR conditions: modulation amplitude, 20 G; modulation frequency, 100 kHz; microwave frequency, 9.42 GHz; microwave power, 5 mW; temperature, 9 K.

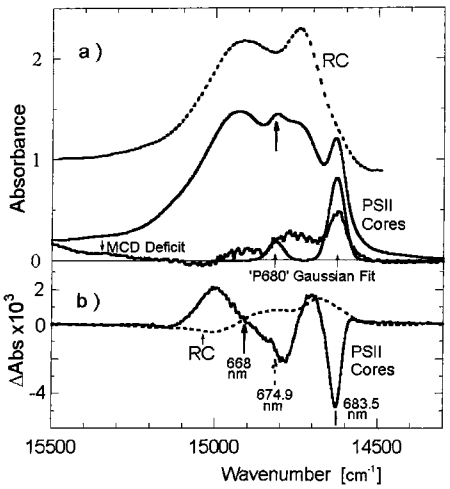

FIGURE 6: (a) Comparison of chl Q_y region for PSII core complexes (this work) and a typical D1/D2/b_{559} preparation (*38*). Inequivalent vertical scales. With the core complex spectrum are shown the scaled MCD deficit spectrum from Figure 3b (absorbance minus monomer-scaled MCD intensity, see text) and two equal-width (45 cm^{-1}) Gaussian bands centered at 14 630 cm^{-1} (683.5 nm) and 14 817 cm^{-1} (674.9 nm), which are fits to the partially resolved features in the core complex absorption envelope assigned to the $Q_y^{\pm}$ components of the exciton split P680 pair (see text). The total area of the 14 630 cm^{-1} Gaussian corresponds to 2.2 chl *a*, assuming the extinction scale from Figure 2a. The midpoint of the $Q_y^{\pm}$ components, 14 724 cm^{-1} (679.2 nm, i.e., the mean apparent monomer transition energy), is very close to the P680 band center seen in D1/D2/b_{559} by absorption, MCD, and triplet-minus-singlet difference spectra (*38*, *44*, *60*). The exciton splitting, ~190 cm^{-1}, is close to the estimated width (~200 cm^{-1}) of the single, inhomogeneously broadened P680 band seen at 4 K in D1/D2/b_{559} by hole-burning (*38*). (b) Comparison of CD spectra for the samples from (a). The relative scaling of the CD to absorbance is the same for the core complexes and D1/D2/b_{559}. Arrows indicate the approximate centers for the broad ~670 nm Gaussian band assigned to mainly CP43, CP47 (see text), and the small positive CD feature corresponding to the 674.9 nm band inferred in (a) (see text).

generates a multiline signal that is very similar to that seen in PSII membranes (*35*). Integration (see Materials and Methods) of this signal indicates that approximately 1 spin = 1/2 center has been formed per 32 chl (i.e., per RC). NIR illumination of PSII poised in the S_2 spin = 1/2 state giving rise to the multiline signal converts the Mn center into the higher spin state giving rise to the $g \approx 4.1$ signal (*51*, *52*). Figure 5 shows that this procedure works efficiently in the PSII core complex material, with 40−70% NIR-induced interconversion between the multiline and $g \approx 4.1$ states being achievable at 140 K illumination. No clear evidence is seen for the signals at higher g ($g \approx 8-10$) reported for NIR illumination below 150 K (*52*).

Although the EPR characterization given here is for PSII material glassed in the polyalcohol cryoprotectant medium (40%) necessary for the optical studies, essentially the same behavior is seen for the cytochrome and Mn signals when the complexes are frozen in 0.4 M sucrose buffer (not shown). The metal centers (particularly Mn) appear to become perturbed only at polyalcohol levels above ~50% v/v.

DISCUSSION

The recent medium-resolution structural determination of the PSII membrane complex from cyanobacteria (*20*) is expected to significantly advance our understanding of this photosystem. However, many issues with respect to function remain to be clarified. Also, PSII derived from eukaryotes or higher plants may differ in a number of significant ways from cyanobacterial PSII. In addition to the gross differences associated with the light-harvesting and Mn-stabilizing extrinsic proteins, it is likely that there are significant differences, at the detailed structural level, between the reaction center pigment organization in the two systems (see below). Magnetic interactions within the catalytic site Mn clusters may also differ.

In terms of spectral detail, the present material provides the most detailed 'view' yet obtained for intact, oxygen-evolving PSII from any source. Figure 6 shows a comparison of the chl *a* Q_y regions for the PSII core complexes and typical spectra for D1/D2/b_{559} material from the literature (*38*). In Figure 6a, the scaled MCD deficit (total absorbance minus MCD intensity, scaled for monomeric chl *a* as previously outlined) from Figure 3b is shown, as well as a least-squares fit to a Gaussian of the distinct 14 630 cm^{-1} feature in the core complex. We can discern several components in the Q_y region of the spectra:

(1) The MCD deficit is significant only below ~14 900 cm^{-1} (>670 nm), indicating substantial coupling between the pigments in this region. This is the region also exhibiting the most structured absorbance and CD behavior. This region

is most likely dominated by the more strongly coupled reaction center pigments.

(2) The CD spectrum, which is featureless in the range 16 000−21 000 cm^{-1}, is intense and close to conservative in the Q_y region. This is expected if exciton coupling is the principal mode of pigment interaction in the core complexes and that this process dominates the CD. The CD of monomeric chl *a* is weak, negative, and closely follows the absorption shape with $\Delta\epsilon_{max}/\epsilon_{max} = -0.16 \times 10^{-3}$ (*53*). In the blue region (above 14 700 cm^{-1}) of the core complex spectrum, which consists mainly of a broad, quasi-Gaussian absorption feature [center ∼14 930 cm^{-1} (670 nm), width ∼250 cm^{-1}], the CD has a maximum CD/peak absorption, $|\Delta\epsilon_{max}/\epsilon_{max}|$, of $\sim 2 \times 10^{-3}$. The near to simple derivative shape is similar to that observed in light-harvesting proteins (*54*). The CD zero crossing is only slightly red-shifted (∼10−20 cm^{-1}) from the maximum. This may indicate that the spectroscopic environment of the responsible chromophores is similar (*54*). The broad Gaussian accounts for ∼70% of the total Q_y intensity. We assign it to be, principally, the CP47 and CP43 inner light-harvesting proteins in the assembled complex.

There are literature reports of CD from oxygen-evolving PSII material [cores and BBY (*55*), and chloroplast fragments (*56*)]. These spectra have some similarity to those of the present core preparation, with a prominent negative feature around 14 600 cm^{-1} and a positive feature near 15 000 cm^{-1}, but they also have marked features below 16 000 cm^{-1} (*55*), where our material shows no CD. The reported CD spectra from isolated CP43 (*39*) and CP47 (*40*), when added, resemble the present core complex Q_y CD in the blue region (above 14 700 cm^{-1}) but differ significantly in the red region, lacking the intense 14 630 cm^{-1} feature.

(3) There is a significant absorbance tail to the red of the 14 630 cm^{-1} band. This corresponds to ∼1 chl centered at ∼14 600 cm^{-1} (685 nm) with peak width <100 cm^{-1}. This band does not exhibit an MCD deficit and so appears not to be part of any strongly coupled system. Bands corresponding to 1−2 chl in total intensity have been observed in this region for isolated CP47 (*41*).

The Spectroscopic Signature of P680. Within the spectral region assigned to the reaction center pigments (those displaying an MCD deficit, Figure 3b), the most prominent feature is the peak at 14 630 cm^{-1} (683.5 nm). The band area of the Gaussian fit to this absorption peak corresponds to 2.2 chl *a* in total $Q_y(0,0)$ dipole strength, and has a width of only 45 cm^{-1}. Two recent results from intact PSII systems include both P680 triplet-minus-singlet and $P680^+Pheo^-$ − P680Pheo difference spectra (*57*−*59*). These show a bleaching band at 684−685 nm, centered at the same wavelength as the strong 683.5 nm feature seen here. The line width obtained from the $P680^+Pheo^-$ − P680Pheo bleaching in (*58*) (∼60 cm^{-1}) is also comparable to that which we observe, although the line width obtained from the triplet difference spectra (*57, 58*) is somewhat greater.

We can then associate the clearly resolved absorption feature in Figure 6 with P680 in higher plants. The total oscillator strength of ∼2.2 chl *a* equiv suggests that at least 2 chl *a* are involved.

As mentioned previously, the MCD deficit at the 14 630 cm^{-1} (683.5 nm) feature is ∼50%. We note that the special pair reaction center dimers of PSI (P700), purple bacteria (P850), and PSII in the form of D1/D2/b_{559} complexes (possibly perturbed P680) each exhibited B_0/D_0 values close to half the respective monomer values. Phenomenologically, this deficit is a signature of interchromophore coupling. Nozawa and colleagues have shown (*44, 60*) that the B_0/D_0 for bacteriochlorophyll in solution is dependent on the degree of aggregation. For dimers, the B_0/D_0 value was 50% of the monomer value, becoming progressively less in higher aggregate (trimer, tetramer) forms. Assuming that the MCD deficit of the P680 pigments arises from interchromophore coupling, the 50% MCD value observed implies predominantly *pairwise* coupling within the P680 moiety.

We are presently engaged in a detailed theoretical study of the spectral consequences of a pigment interaction scheme dominated by an exciton-coupled special pair. One interesting preliminary finding (J. L. Hughes et al., in preparation) is that couplings between the central chlorophylls and each of the accessory chl pigments can be as large as ∼30% of the special pair coupling (i.e., ∼30 cm^{-1}), *without* significantly perturbing the dimer-like spectral appearance of the central pair. Given the characteristic geometry of the pigments in PSII reaction centers, such secondary interactions are almost certainly present (*61*). These secondary interactions will be strongly modified by the formation of the P680 triplet state. The triplet state is reported to be localized on the accessory chl (*38, 62*). It may be possible to rationalize the triplet state bleaching observed at 684−685 nm by considering these secondary interactions.

From the above, we take that, to a first approximation, P680 is dominated by an exciton-coupled dimer analogous to the bacterial RC dimer (P850). The intense lower component of the split pair (Q_{y^-}) is at 14 630 cm^{-1} (683.5 nm) and has an intensity roughly twice that of a chl *a* monomer. For the expected geometry of P680 (closely antiparallel), theory requires the blue-shifted component of the exciton split Q_y band (Q_{y^+}) to have low intensity. This feature should have opposite CD but similar width to the allowed band.

A plausible candidate for the Q_{y^+} transition in the absorbance and CD data is visible at 14 817 cm^{-1} (674.9 nm), which is indicated in Figure 6a,b. The band is of similar width (∼50 cm^{-1}), with an intensity in absorbance ∼20% of that for the 14 630 cm^{-1} band and a position at the blue edge of the MCD deficit region. The exciton coupling constant inferred from the spacing is ∼94 cm^{-1}.

The assignment of the bands at 14 630 and 14 817 cm^{-1} to strongly interacting pigments within the P680 system is further supported by recent studies in our laboratories (*37*) of electrochromic band shifts following functional turnover ($S_1 \rightarrow S_2$) in the PSII core complexes. These experiments show the pigments giving rise to the 14 630 and 14 817 cm^{-1} bands to be *close* to the catalytic Mn site in the D1 protein and that the two bands respond *equivalently* to charge movements associated with S-state turnover.

Applying the transition point dipole model [e.g., (*53*)] to the observed exciton coupling (94 cm^{-1}) of the pair, the chl center-to-center separation in the plant special pair is 11−12 Å, slightly longer than the value of 10.0 Å observed in cyanobacteria (*20*).

The CD of the 14 630 cm^{-1} band is the most intense in the region, with $\Delta\epsilon_{max}/\epsilon_{max} = -4.0 \times 10^{-3}$. The 14 817 cm^{-1} band has associated a positive CD component of appropriate

width, but much smaller amplitude than the strong negative band at 14 630 cm^{-1}. Phenomenologically, such pronounced CD nonconservation (asymmetry) in the Q_y region of chl systems can be associated with dimerization, or higher oligomer formation (*53, 63*−*65*). Simple exciton coupling theory [e.g., (*54*)] does not predict such an effect, but chromophore interaction-induced mixing of higher energy states (Q_x, $B_{x,y}$, etc) into the Q_y levels can induce CD asymmetry in the Q_y region (*63, 64*). However, for this effect to be substantial, the exciton coupling has to be large (hundreds of cm^{-1}) to induce the necessary mixing. This is essentially excluded by the narrowness of the PSII core complex Q_y envelope. Further, the CD is still conservative overall, when all transitions are considered. That is, CD asymmetry in the Q_y region is balanced by correspondingly intense, complementary CD asymmetries in the Q_x, B transitions, etc.

We see no evidence of this, with weak to negligible CD at higher energies. Parallel behavior is seen for some model chl oligomer systems exhibiting comparably intense CD asymmetry in the Q_y region (*65*). One possible explanation is that structural effects (such as Mg ligation) arising from close chromophore association induce a large change in the nonconservative, intrinsic CD of the Q_y transitions of the interacting chromophores. There is evidence that specific chlorin−protein interactions in bacterial reaction centers produce similar effects (*66*).

The CD of a single chromophore may be strongly influenced by its environment in a protein, which may *include* a structural influence associated with neighboring chromophores. These changes may compete with or disguise the excitonic CD effects usually discussed.

Comparison with Solubilized D1/D2/Cyt b_{559} Material. As is evident from the comparison in Figure 6, spectral features in the reaction center region of the cores do not have a 1:1 correspondence with the spectra reported for isolated D1/D2/b_{559}. The reported CD spectra of these preparations are inverted with respect to those observed here. Our spectra have the same sign as those of earlier, more intact preparations (*55*, *56*). This, combined with the variability of optical spectra reported with varying detergent treatments (*31*), suggests a significant perturbation of the chromophore interactions in D1/D2/b_{559} preparations, compared to the intact reaction center.

The reaction center region absorption envelope in functional PSII cores is narrower and red-shifted compared to the spectrum of D1/D2/b_{559} particles. We take this as evidence for substantial changes in both coupling and environment of the reaction center pigments.

D1/D2/b_{559} spectra show a weak shoulder near the position of the prominent P680 feature of the intact system. Whether this represents a minor population with 'intact' P680 chromophore geometry (see Figure 6) or some other component is as yet unclear.

Comparison with Cyanobacterial PSII. The absorption envelope of the intact PSII core in higher plants is substantially different from that in cyanobacteria. This is evident in 77 K spectra (*67*) but especially so in 4 K spectra (V. M. Masters et al., unpublished work). The difference is most pronounced near the red edge of the Q_y envelope and may reflect a significant difference of the P680 organization in plants and cyanobacteria, as discussed above. However, low-temperature single-turnover studies on our plant PSII samples (*37*) show that bands involving the active branch pheophytin have very similar location and electrochromic response to those in cyanobacteria (*67*).

PSII Stoichiometry. The higher plant core complex presented here contains 4.5 Mn per 32 chlorophylls (1 Mn per 7.1 chl *a*). While a value of 4 Mn per reaction center of PSII is widely accepted, the literature data are, in fact, more equivocal. The early studies involving PSII fractions from higher plants [reviewed in (*7*)] suffered uncertainties concerning the fraction of total sample Mn assignable to the water splitting site. The precise chl-to-reaction center ratio in detergent-solubilized systems also suffered uncertainties.

Purified, active PSII core complexes from cyanobacteria have been available for over a decade, but the reported chl per Mn in these systems has always exceeded ∼11 and has an average of ∼15 (*7, 8, 10, 14*). Given that the cyanobacterial and higher plant PSII core complexes are now known to have very similar chl contents (32−34 chl *a* per reaction center), this result is puzzling, as the reported Mn content and specific catalytic activity show no obvious correlation for the cyanobacterial preparations. The total electron density volume assigned to Mn in the recently reported structure of PSII from thermophillic bacteria (*20*) is consistent with a Mn per reaction center stoichiometry greater than the value of 2 suggested by a chl/Mn ratio of 15.

The stoichiometry of cyt b_{559} per PSII and indeed the exact function of the cytochrome unit itself have long been under discussion. The quoted range for cyt b_{559} content in PSII is 1−2 per photosystem monomer [e.g., see (*68*)]. A value of 1 is confirmed for the cyanobacterial PSII core complex, by crystallography (*20*). This is also the value we find in the higher plant complex.

From densitometric scans of the gel patterns, we find essentially the same (within 20% uncertainty) stoichiometry of the cyt b_{559} α-subunit band (relative to the D1/D2, CP47, CP43 peptides) in PSII core complexes and the PSII membrane particles from which the complexes were made. This is confirmed by the MCD determination of the total cyt b_{559} signals from PSII particles. Our approach to the cyt b_{559} stoichiometry problem is novel and avoids some of the difficulties inherent in analytical procedures previously employed [see discussion in (*68*)]. We feel that a stoichiometry of 1.0 cyt b_{559} per reaction center is the correct figure for PSII-enriched particles derived from spinach, although the average stoichiometry for the whole thylakoid membrane is not addressed in our studies.

ACKNOWLEDGMENT

We are extremely grateful to T. Hundall and C. Spetea (Linköping University, Sweden) for quantitative gel scans and western blotting data on our photosystem samples.

REFERENCES

1. Bricker, T. M. (1990) *Photosynth. Res. 24*, 1−13.
2. Svensson, B., Vass, I., and Styring, S. (1991) *Z. Naturforsch. 46C*, 765−776.
3. Barber, J., Nield, J., Morris, E. P., Zheleva, D., and Hankamer, B. (1997) *Physiol. Plant. 100*, 817−827.
4. Woollman, F.-A., Minai, L., and Nechushtai, R. (1999) *Biochim. Biophys. Acta 1411*, 21−85.
5. Debus, R. J. (1992) *Biochim. Biophys. Acta 1102*, 269−352.

6. Glazer, A. N. (1994) *J. Appl. Phycol. 6*, 105−112.
7. Pauly, S., and Witt, H. T. (1992) *Biochim. Biophys. Acta 1099*, 211−218.
8. Noren, G. H., Boerner, R. J., and Barry, B. A. (1991) *Biochemistry 30*, 3943−3950.
9. van Leeuwen, P. J., Nieveen, M. C., van de Meent, E. J., Dekker, J. P., and van Gorkom, H. J. (1991) *Photosynth. Res. 28*, 149−153.
10. Tang, X.-S., and Diner, B. A. (1994) *Biochemistry 33*, 4594−4603.
11. Roobol-Bóza, M., and Andersson, B. (1996) *Anal. Biochem. 235*, 127−133.
12. Hankamer, B., Nield, J., Zheleva, D., Boekema, E., Jasson, S., and Barber, J. (1997) *Eur. J. Biochem. 243*, 422−429.
13. Bricker, T. M., Morvant, J., Masri, N., Sutton, H. M., and Frankel, L. K. (1998) *Biochim. Biophys. Acta 1409*, 50−57.
14. Reifler, M. J., Chisholm, D. A., Wang, J., Diner, B. A., and Brudvig, G. W. (1998) in *Photosynthesis: Mechanisms and Effects* (Garab, G., Ed.) pp 1189−1192, Kluwer Academic Publishers, Dordrecht, The Netherlands.
15. Sugiura, M., Minagawa, J., and Inoue, Y. (1999) *Plant Cell Physiol. 40*, 311−318.
16. Sugiura, M., and Inoue, Y. (1999) *Plant Cell Physiol. 40*, 1219−1231.
17. Kuhl, H., Kruip, J., Seidler, A., Krieger-Liszkay, A., Bünker, M., Balk, D., Scheidig, A. J., and Rögner, M. (2000) *J. Biol. Chem. 275*, 20652−20659.
18. Shen, J.-R. (2000) *Biochemistry 39*, 14739−14744.
19. Zouni, A., Jordan, R., Schlodder, E., Fromme, P., and Witt, H. T. (2000) *Biochim. Biophys. Acta 1457*, 103−105.
20. Zouni, A., Witt, H.-T., Kern, J., Fromme, P., Kraub, N., Saenger, W., and Orth, P. (2001) *Nature 409*, 739−743.
21. Eshaghi, S., Andersson, B., and Barber, J. (1999) *FEBS Lett. 446*, 23−26.
22. Rhee, K.-H., Morris, E. P., Barber, J. A., and Kühlbrandt, W. (1998) *Nature 396*, 283−286.
23. Barber, J., Morris, E., and Büchel, C. (2000) *Biochim. Biophys. Acta 1459*, 239−247.
24. Michel, H., and Deisenhofer, J. (1988) *Biochemistry 27*, 1−7.
25. Svensson, B., Etchebest, C., Tuffery, P., van Kan, P., Smith, J., and Styring, S. (1996) *Biochemistry 35*, 14486−14502.
26. Schelvis, J. P. M., van Noort, P. I., Aartsma, T. J., and van Gorkom, H. J. (1994) *Biochim. Biophys. Acta 1184*, 242−250.
27. Durrant, J. R., Klug, D. R., Kwa, S. L. S., van Grondelle, R., Porter, G., and Dekker, J. P. (1995) *Proc. Natl. Acad. Sci. U.S.A. 92*, 4798−4802.
28. Greenfield, S. R., Seibert, M., and Wasielewski, M. R. (1999) *J. Phys. Chem. B 103*, 8364−8374.
29. Jankowiak, R., Rätsep, M., Picorel, R., Seibert, M., and Small, G. J. (1999) *J. Phys. Chem. B 103*, 9759−9769.
30. Nanba, O., and Satoh, K. (1987) *Proc. Natl. Acad. Sci. U.S.A. 84*, 109−112.
31. van der Vos, R., van Leeuwen, P. J., Braun, P., and Hoff, A. J. (1992) *Biochim. Biophys. Acta 1140*, 184−198.
32. Smith, P. J., Ahrling, K. A., and Pace, R. J. (1993) *J. Chem. Soc., Faraday Trans. 89*, 2863−2868.
33. Porra, R. J., Thompson, W. A., and Kriedemann, P. E. (1989) *Biochim. Biophys. Acta 975*, 384−394.
34. Gilmore, A. M., and Yamamoto, H. Y. (1991) *J. Chromatogr. 543*, 137−145.
35. Smith, P. J., and Pace, R. J. (1996) *Biochim. Biophys. Acta 1275*, 213−220.
36. Stranger, R., Dubicki, L., and Krausz, E. (1996) *Inorg. Chem. 35*, 4218−4226.
37. Masters, V. M., Smith, P. J., Krausz, E., and Pace, R. J. (2001) *J. Lumin.* (in press).
38. Kwa, S. L. S., Eijckelhoff, C., van Grondelle, R., and Dekker, J. P. (1994) *J. Phys. Chem. 98*, 7702−7711.
39. Groot, M.-L., Frese, R. N., de Weerd, F., Bromek, K., Pettersson, Å., Peterman, E. J. G., van Stokkum, I. H. M., van Grondelle, R., and Dekker, J. P. (1999) *Biophys. J. 77*, 3328−3340.
40. van Dorssen, R. J., Breton, J., Plijter, J. J., Satoh, K., van Gorkom, H. J., and Amesz, J. (1987) *Biochim. Biophys. Acta 893*, 267−274.
41. Alfonso, M., Montoya, G., Cases, R., Rodriguez, R., and Picorel, R. (1994) *Biochemistry 33*, 10494−10500.
42. Chang, H. C., Jankowiak, R., Yocum, C. F., Picorel, R., Alfonso, M., Seibert, M., and Small, G. J. (1994) *J. Phys. Chem. 98*, 7717−7724.
43. Piepho, S. B., and Schatz, P. N. (1983) *Group Theory in Spectroscopy, with Applications to Magnetic Circular Dichroism*, Wiley, New York.
44. Kobayashi, M., Wang, Z.-Y., Yoza, K., Umetsu, M., Konami, H., Mimuro, M., and Nozawa, T. (1996) *Spectrochim. Acta, Part A 51*, 585−598.
45. Cheesman, M. R., Greenwood, C., and Thomson, A. J. (1991) *Adv. Inorg. Chem. 36*, 201−255.
46. Sievers, G., Gadsby, P. M. A., Peterson, J., and Thomson, A. J. (1983) *Biochim. Biophys. Acta 742*, 637−647.
47. Foote, N., Peterson, J., Gadsby, P. M. A., Greenwood, C., and Thomson, A. J. (1984) *Biochem. J. 223*, 369−378.
48. Moore, G. R., Williams, R. J. P., Peterson, J., Thomson, A. J., and Mathews, F. S. (1985) *Biochim. Biophys. Acta 829*, 83−96.
49. Ahrling, K. A., and Styring, S. (2000) in *Probing Photosynthesis—Mechanisms, Regulation and Adaptation* (Yunus, M., Pathre, U., and Mohanty, P., Eds.) pp 148−163, Taylor and Francis, London.
50. Miller, A.-F., and Brudvig, G. W. (1991) *Biochim. Biophys. Acta 1056*, 1−18.
51. Boussac, A., Girerd, J.-J., and Rutherford, A. W. (1996) *Biochemistry 35*, 6984−6989.
52. Boussac, A., Un, S., Horner, O., and Rutherford, A. W. (1998) *Biochemistry 37*, 4001−4007.
53. Houssier, C., and Sauer, K. (1970) *J. Am. Chem. Soc. 92*, 779−791.
54. Koolhaas, M. H. C., van der Zwan, G., Frese, R. N., and van Grondelle, R. (1997) *J. Phys. Chem. B 101*, 7262−7270.
55. van Dorssen, R. J., Plijter, J. P., Dekker, J. P., den Ouden, A., Amesz, J., and van Gorkom, H. J. (1987) *Biochim. Biophys. Acta 890*, 134−143.
56. Canaani, O. D., and Sauer, K. (1978) *Biochim. Biophys. Acta 501*, 545−551.
57. Carbonera, D., Giacometti, G., and Agostini, G. (1994) *FEBS Lett. 343*, 200−204.
58. Hillmann, B., Brettel, K., van Mieghem, F., Kamlowski, A., Rutherford, A. W., and Schlodder, E. (1995) *Biochemistry 34*, 4814−4827.
59. van Mieghem, F., Brettel, K., Hillmann, B., Kamlowski, A., Rutherford, A. W., and Schlodder, E. (1995) *Biochemistry 34*, 4798−4813.
60. Nozawa, T., Kobayashi, M., Wang, Z.-Y., Itoh, S., Iwaki, M., Mimuro, M., and Satoh, K. (1995) *Spectrochim. Acta, Part A 51*, 125−134.
61. Dekker, J. P., and van Grondelle, R. (2000) *Photosynth. Res. 63*, 195−208.
62. van Mieghem, F. J. E., Satoh, K., and Rutherford, A. W. (1991) *Biochim. Biophys. Acta 1058*, 379−385.
63. Scherz, A., and Parson, W. W. (1984) *Biochim. Biophys. Acta 766*, 666−678.
64. Koolhaas, M. H. C., van der Zwan, G., van Mourik, F., and van Grondelle, R. (1997) *Biophys. J. 72*, 1828−1841.
65. Tamiaki, H., Kubo, M., and Oba, T. (2000) *Tetrahedron 56*, 6245−6257.
66. Mar, T., and Gingras, G. (1995) *Biochemistry 34*, 9071−9078.
67. Stewart, D. H., Nixon, P. J., Diner, B. A., and Brudvig, G. W. (2000) *Biochemistry 39*, 14583−14594.
68. Stewart, D. H., and Brudvig, G. W. (1998) *Biochim. Biophys. Acta 1367*, 63−87.
69. Zheleva, D., Sharma, J., Panico, M., Morris, H. R., and Barber, J. (1998) *J. Biol. Chem. 273*, 16122−16127.

BI0111202